

EIGENVECTOR 1: AN OPTIMAL CORRELATION SPACE FOR ACTIVE GALACTIC NUCLEI

J. W. Sulentic¹, T. Zwitter², P. Marziani³ and D. Dultzin-Hacyan⁴

Subject headings: Galaxies: Seyfert – Galaxies: Quasars – Line: Formation – Line: Profiles

ABSTRACT

We identify a correlation space involving optical and UV emission line parameters as well as the soft X-ray spectral index that provides optimal discrimination between all principal classes of active galactic nuclei. Most of the sources in our three high quality data samples show a strong intercorrelation with narrow line Seyfert 1 (NLSy1) galaxies and steep spectrum radio galaxies occupying opposite extrema in the space. NLSy1 sources show a clear continuity with broader line sources indicating that they are not a disjoint class of AGN as is sometimes suggested. We interpret the principal intercorrelation in the parameter space as being driven by AGN luminosity to black hole mass ratio ($L/M \propto$ Eddington ratio). Source orientation no doubt also plays an important role but it is not yet clear whether FWHM $H\beta$ or $CIV\lambda 1549$ line shift is the better indicator. We tentatively identify two RQ populations: an almost pure RQ population A with $FWHM \leq 4000$ and population B which occupies the same parameter domain as the flat spectrum RL sources. A possible interpretation sees Pop. A/NLSy1 as lower mass/high accretion rate sources and Pop. B/RL sources the opposite.

1. Introduction

The search for correlations among observational parameters that describe AGN has been developing rapidly in the past few years. At the same time there has been a theoretical countercurrent that views all quasar spectra as remarkably similar. This erroneous view is due in part to the low resolution and s/n of much available spectral data. Blurred quasar spectra do look remarkably similar but data with $s/n > 20$ in the continuum and resolution $\sim 5\text{\AA}$ show striking differences from which a pattern is beginning to emerge. Some of the most promising correlations arose when high s/n optical spectra were published for the lower redshift ($z \lesssim 0.5$) sources in the Bright Quasar Survey (Boroson & Green 1992: BG92). A principal component analysis of the BG92 correlation matrix showed “eigenvector 1” correlations involving the widths and strengths of $[OIII]\lambda 5007$, as well as broad $H\beta$ and $FEII_{opt}$ emission lines. More recently measures of X-ray luminosity, particularly the soft X-ray photon index, have emerged as a related part of the eigenvector 1 correlations (Wang, Brinkmann & Bergeron 1996).

We report a study of correlations involving the best available data samples for low redshift ($z \lesssim 1.0$) Active Galactic Nuclei (AGN). We find a correlation space where we are able to discriminate between all of the major forms of AGN phenomenology (e.g. broad and narrow Line Seyfert 1 galaxies, regular and

¹Department of Physics and Astronomy, University of Alabama, Tuscaloosa, AL 35487; giacomom@merlot.astr.ua.edu

²Department of Physics, University of Ljubljana, Jadranska 19, 1000 Ljubljana, Slovenia; tomaz.zwitter@uni-lj.si

³Osservatorio Astronomico di Padova, vicolo dell’Osservatorio 5, I-35122 Padova, Italy; marziani@pd.astro.it

⁴Instituto de Astronomia, UNAM, Mexico, DF 04510, Mexico; deborah@astroscu.unam.mx

broad absorption line (BAL) quasars, steep and flat spectrum broad line radio galaxies). We refer to it as the Eigenvector 1 (hereafter E1) space reflecting its partial roots in the BG92 study. The three principal “orthogonal” correlates involve measures of: 1) low ionization broad line width - full width at half maximum of $H\beta$ ($\text{FWHM } H\beta_{\text{BC}}$), 2) ratio of line strengths - the continuum normalized ratio of the optical FeII_{opt} and broad $H\beta$ emission line strengths ($R_{\text{FeII}} = W(\text{FeII } \lambda 4570 \text{ blend})/W(H\beta_{\text{BC}})$) and 3) X-ray continuum strength - the soft X-ray photon index (Γ_{soft}). Parts of this correlation space have been discussed for almost ten years (e.g. Boroson & Green 1992 (PG92); Boller et al. 1996; Marziani et al. 1996 (MS96); Wang et al., 1996; Laor et al. 1997) but the pieces have not previously been united in this way. We present the basic E1 phenomenology in this paper. In a following paper we will consider the principal physical drivers of the E1 correlations.

2. The E1 Correlation Space

Figures 1 a,b,c show the 2D projections of the E1 correlation space. AGN plotted in the figures come from three data sources: 1) the BG92 sample of 87 mostly radio-quiet (RQ) AGN (16 radio-loud: RL), 2) the MS96 mixed sample of 21 RQ and 31 RL sources as well as 3) a sample of 24 new sources with matching HST UV archival and optical ground-based spectra (8 RL). The data sources combine the most complete sample of AGN with high quality spectral data (BG92) and two overlapping samples of comparable quality data with matching optical $H\beta$ and UV $\text{CIV } \lambda 1549$. Soft X-ray photon indices are available for a large fraction of the above samples (Wang et al. 1996; Brinkmann et al. 1997; Siebert et al. 1998; Yuan et al. 1998). Values determined with hydrogen column density N_H as a free parameter were preferred when available. The hard X-ray photon index provides an alternative, but less sensitive, E1 correlate (Piccinotti et al. 1982; Brandt et al. 1997). Our total sample includes 128 sources (45 RL) with optical measures, of which, 76 (39 RL) have UV measures. Mean error bars (2σ) are indicated with: i) average errors for sources in the middle of the diagrams for $\text{FeII } \lambda 4570$ and $H\beta$ measures as well as ii) a median value for all Γ_{soft} measures. See BG92 and MS96 for detailed discussion of reduction and analysis procedures.

RQ sources are indicated by solid symbols in the figures while open and crossed circles indicate flat (core-dominated) and steep (lobe-dominated) spectrum RL (as defined by Kellermann et al 1989) sources respectively. The majority of sources show a well defined correlation in Figures 1 a,b,c. One can make a first order interpretation of E1 correlations in terms of RL vs. RQ differences. Sources that fall in the large $\text{FWHM } H\beta$ and large R_{FeII} region (like PG 0043+039; Turnshek et al 1994) are apparently very rare and pathological (possibly associated to mixed Starburst/AGN properties). Fig. 1 a,b,c indicate that these two populations show a clear separation with RQ having, for example, a mean $\text{FWHM}(H\beta_{\text{BC}}) \approx 2300 \text{ km s}^{-1}$ less than RL sources (a few RL sources with $\text{FWHM}(H\beta_{\text{BC}}) \sim 11\text{--}20000 \text{ km s}^{-1}$ are not shown in the figures). An alternative interpretation of E1 sees two populations of RQ AGN: 1) population A (filled boxes) which shows little overlap with the RL domain (65% of the BG92 RQ sample) and 2) population B (filled circles) that occupies essentially the same E1 domain as the RL sources (25% of the BG92 RQ sources). Fig. 1 d shows a plot of $W(\text{FeII } \lambda 4570)$ vs. $\text{FWHM}(H\beta_{\text{BC}})$ for the BG92 sample that provided the motivation for the population A–B concept. Rather than a correlation this plot shows two disjoint populations of sources with no correlation within either population. Correlations appear when R_{FeII} is used instead of $W(\text{FeII}_{\text{opt}})$ or $W(H\beta_{\text{BC}})$. We introduce the population A and B distinction for the sake of argument but suggest that it may have more fundamental significance. Table 1 presents mean parameter values (and associated sample standard deviations) in arbitrary bins of $\text{FWHM}(H\beta_{\text{BC}})$ that allow one to compare RL vs. RQ as well as Pop. A vs. Pop. B sources.

It is not easy at this time to determine what role sample selection biases play in E1 but it is clear that BG92 selection techniques favored RQ sources with narrow Balmer line profiles. Recent work indicates that selection on the basis of soft X-ray excess favors them even more strongly (e.g. Moran et al. 1996; Grupe et al. 1999). At the same time core-dominated/flat spectrum RL sources are no doubt over-represented if their emission is beamed. This study makes no claim to completeness. Beyond BG92 our sample selection is driven by the availability of i) high s/n and resolution ground based data and ii) matching HST UV spectra. Table 2 presents the results of a correlation analysis for the three principal E1 and related parameters (the Pearson’s correlation coefficient r_P is reported along with the probability P of a chance correlation in a sample of N objects). As the figures and Table 2 also suggest, the strongest E1 correlations are found for the RQ sources. The highest ranked E1 correlation (Γ_{soft} vs. FWHM $H\beta_{\text{BC}}$) is present only in the RQ sample which is not surprising since RL sources show no evidence for a soft X-ray excess. The nearly identical r_P for the ALL RQ and Pop. A RQ samples suggest that the principal correlations are driven by Pop. A. RQ Pop. B and RL sources show the same E1 parameter domain and neither sample shows evidence for significant internal correlations. The latter result is due, at least in part, to: a) the absence of a soft X-ray excess in these sources and b) the weakness of FeII_{opt} emission in these relatively broad-lined sources. If the minimum detectable FeII_{opt} emission for sources with profile widths $\text{FWHM}(\text{FeII } \lambda 4570) \approx \text{FWHM}(H\beta_{\text{BC}}) \approx 1000 \text{ km s}^{-1}$ is $W(\text{FeII } \lambda 4570) \approx 10\text{--}15 \text{ \AA}$ then we estimate that it will be ≈ 25 and 40 \AA for $\text{FWHM}(H\beta_{\text{BC}}) \approx 5000$ and 10000 km s^{-1} , respectively. The message here is that values of $R_{\text{FeII}} \lesssim 0.2$ are very uncertain even with the best available data.

There are several lines of evidence that suggest continuum luminosity is uncorrelated with E1 parameter space. 1) Optical luminosity appears in the second orthogonal eigenvector identified in BG92, 2) BAL sources occupy a similar domain to the NLSy1 but they are “displaced” in: a) X-ray luminosity - BALs are X-ray quiet and b) optical luminosity where they are on average about $4\times$ more luminous than the NLSy1 sources in BG92. 3) RL and Pop. B RQ sources occupy the same parameter domain but the RL sources show $\sim 5\times$ higher optical continuum luminosities which may in part reflect the presence of beamed sources in the RL sample. 4) We also find no evidence for a correlation between E1 coordinates and radio continuum luminosity for RQ sources (see Kellermann et al. 1989; Falcke et al. 1996). This last result tells us that RL sources are a distinct AGN population that shows fundamental differences in BLR structure and kinematics. E1 indicates that the weak radio emission from RQ sources is unrelated to the RL phenomenon.

E1 also shows evidence for a parameter space separation between steep and flat spectrum RL sources. This shows up in Table 2 as a possible RL correlation between FWHM $H\beta_{\text{BC}}$ and R_{FeII} . Steep spectrum RL sources represent the opposite extremum from NLSy1 while flat spectrum sources are more similar to RQ sources. The tendency for steep spectrum RL sources to show the broadest Balmer profiles and the weakest FeII_{opt} emission is confirmed in two large (with some source overlap between themselves and our RL sample) surveys (Brotherton 1996; Corbin 1997). Siebert et al (1998) provide evidence that this separation may also be present in the X-ray spectral index. NLSy1 are a RQ and population A extremum with the narrowest Balmer line profiles, strong FeII_{opt} emission and a strong soft X-ray excess. NLSy1 show a clear continuity and correlation with broader line Seyfert 1 galaxies in all measured parameters. This challenges the idea that they represent a unique or disjoint AGN population. BAL quasars (4 RQ BAL in the BG92 sample) occupy an E1 domain that is similar to the NLSy1. Other (BAL) studies (e.g. Boroson & Myers 1992) have also suggested that BAL quasars show Balmer line $\text{FWHM} \lesssim 3000 \text{ km s}^{-1}$ and moderate to strong R_{FeII} measures.

Much less clear is whether RQ population B sources represent a disjoint AGN population or show a smooth continuation of the population A correlations. Figure 1 b for example shows a breakdown of

the $\Gamma_{\text{soft}} - \text{FWHM}(\text{H}\beta)$ correlation at the nominal boundary between population A and B. Whatever the relation between the two RQ populations, their line profiles show striking differences. Figure 2 shows a comparison of the $\text{H}\beta_{\text{BC}}$ and $\text{CIV}\lambda 1549_{\text{BC}}$ line profiles for prototype NLSy1 source I Zw 1 and NGC 5548 which is a typical broad line Seyfert galaxy. While differences in the Balmer profiles are striking, the most impressive difference is the apparent kinematic *decoupling* of the $\text{CIV}\lambda 1549$ and $\text{H}\beta$ profiles in I Zw 1. Our previous work (MS96) suggested that properly NLR corrected $\text{CIV}\lambda 1549$ in RQ sources (see Sulentic & Marziani 1999) is always blueshifted relative to $\text{H}\beta$ and the AGN rest frame. Fig. 3 shows the $\text{CIV}\lambda 1549_{\text{BC}}$ line shift vs. $\text{FWHM}(\text{H}\beta_{\text{BC}})$ diagram. We have normalized the $\text{CIV}\lambda 1549$ shift by $W(\text{CIV}\lambda 1549)$ in this plot because we see a complementary trend in E1 for $W(\text{CIV}\lambda 1549)$ to be smallest in the NLSy1 population. Figure 3 confirms that essentially all RQ sources show a $\text{CIV}\lambda 1549$ blueshift while RL sources show equal red and blueshifts with amplitudes generally less than $\pm 10^3 \text{ km s}^{-1}$. Correlations of $\text{CIV}\lambda 1549$ shift with R_{FeII} and Γ_{soft} (see Table 2) indicate that it is likely to be an important E1 correlate. We will explore it further in succeeding papers.

3. From Observational to Physical Parameters

E1 correlates AGN spectroscopic data in a way that removes much of the apparent “randomness” of line properties. It also redefines input parameters for photoionization and kinematical models. We have only begun to explore the E1 parameter space and the physics that drives it. Accumulating evidence from numerous studies suggests that the correlations in E1 involve at least two principal independent parameters: the AGN luminosity to black hole mass ratio and the source orientation. The role of Fe abundance, disk magnetic fields and black hole angular momentum are beyond the scope of this introduction to E1.

Available evidence suggests that the central source luminosity to black hole mass ratio L/M may be systematically higher in Pop. A sources (i.e. a higher accretion rate). A role for L/M is supported by: a) the existence of a soft X-ray excess, particularly in NLSy1, that has been related to a higher accretion rate (Pounds et al. 1995) and b) the thermal signature of the disk itself (Page et al. 1999; Puchnarewicz et al. 1998). If the soft X-ray excess is the high energy end of a thermal signature of the accretion disk then a steep rising blue optical continuum (in low z sources) can be interpreted as the low energy end of the “big blue bump”. This would explain why BG92, with quasars selected on the basis of U–B colors, would favor detection of NLSy1. $\text{CIV}\lambda 1549$ shows the largest blueshifts in NLSy1 sources, and the lowest $\text{CIV}\lambda 1549$ W values, both consistent with the idea that the line emission arises in a disk wind (e.g. Murray & Chiang 1997; Bottorff et al. 1997). The observations are consistent with the idea that L/M is only high enough in RQ sources (especially Pop. A) to trigger a radiation pressure driven outflow. The Balmer profiles in Pop. A sources are most easily interpreted as arising in an optically thick illuminated accretion disk (see e.g. Sulentic et al. 1998). RL sources show Balmer lines with *both* large red and blue profile shifts.

RL sources show no evidence for a soft X-ray excess which may reflect a real absence of this component or that it is dominated by a relatively hard component related to X-ray emission related to the radio loudness. We favor the former interpretation because most RQ population B sources also show a soft X-ray deficit. The absence of a soft X-ray component in RL+RQ pop B sources coupled with the absence of the CIV blueshift are consistent with weak or absent disk structure. The broad lines may arise in a biconical structure in many or all of these sources (Marziani et al. 1993; Sulentic et al. 1995). Evidence for a bicone origin of the BLR includes: a) sources with double peaked broad lines (e.g. Sulentic et al. 1995; Eracleous & Halpern 1998), b) sources with single peaked broad lines showing both large red and blue displacements (e.g. Marziani et al. 1983; Halpern et al. 1998), c) sources with a transient BLR (e.g. Storchi-Bergmann et

al. 1993; Ulrich 2000) and spectropolarimetry of a) and b) sources (Corbett et al. 1998).

The E1 parameter space is measuring aspects of both the geometry and kinematic of the broad line region in AGN. The strength of the correlations and reasonable orthogonality of the parameters suggest that a better diagnostic space for AGN is unlikely to be found. Even in the preliminary presentation, E1 allows us to resolve some AGN conundrums. 1) RL sources are found to be an AGN population with fundamental geometrical and kinematic difference from the RQ majority. 2) NLSy1 are found to be an extremum of the RQ population rather than a pathological or disjoint AGN population. 3) If the width of the Balmer lines bear any signature of source orientation then some NLSy1 (at least, I Zw 1) are seen at or near pole-on (face-on accretion disk) orientation, while some BAL QSOs are likely to be misaligned NLSy1. 4) Population B RQ quasars with Balmer lines broader than $\approx 4000 \text{ km s}^{-1}$ may represent a distinct class (RL pre/post cursors) from narrower population A RQ sources. 5) $\text{CIV}\lambda 1549$ line shifts indicate the presence in Pop. A (and possibly Pop. B) RQ sources of an ubiquitous disk outflow/wind.

PM acknowledges financial support from the Italian Ministry of University and Scientific and Technological Research (MURST) through grant Cofin 98-02-32 and from the IA-UNAM where part of this work was done.

4. References

- Boller, T., Brandt, W.N. & Fink, H. 1996, *A&A*, 305, 53
- Boroson, T.A. & Green, R.F. 1992, *ApJS*, 80, 109
- Boroson, T.A. & Myers, K. 1992, *ApJ*, 397, 442
- Bottoff, M., et al. 1997, *ApJ*, 479, 200
- Brandt W.N., Mathur S. & Elvis M. 1997, *MNRAS*, 285, L25
- Brinkmann, W., Yuan, W. & Siebert, J. 1997, *A&Ap*, 319, 413
- Brotherton, M. S. 1996, *ApJS*, 102, 1
- Corbin, M. 1997, *ApJS*, 113, 245
- Eracleous, M. & Halpern, J. 1998, *ApJ*, 505, 577
- Falcke, H., Sherwood, W. & Patnail, A. 1996, *ApJ*, 471, 106
- Grupe, D., et al. 1999, *A&Ap*, 350, 805
- Halpern, J., Eracleous, M. & Forster, K. 1998, *ApL*, 501, 103
- Kellermann, K. et al. 1989, *AJ*, 98, 1195
- Korista, K.T. et al. 1995, *ApJS*, 97, 285
- Laor, A. et al. 1997, *ApJ*, 477, 93
- Marziani, P., et al. 1993, 410, 56
- Marziani, P., Sulentic, J.W., Dultzin-Hacyan, D., Calvani, M. & Moles, M. 1996, *ApJS*, 104, 37
- Moran, E., Halpern, J. & Helfland, D. 1996, *ApJS*, 106, 341
- Murray, N. & Chiang, J. 1997, 474, 91
- Page, M.J. et al. 1999, *MNRAS*, 305, 775
- Piccinotti, G., Mushotzky, R.F., Boldt, E.A., Holt, S.S., Marshall, F.E., Serlemitsos, P.J. & Shafer, R.A. 1982, *ApJ*, 253, 485
- Pounds, K.A., Done, C. & Osborne, J.P. 1995, *MNRAS*, 277, L5
- Puchnarewicz, E.M. et al. 1998, *MNRAS*, 293, L52
- Siebert, J., et al. 1998, *A&Ap*, 301, 261
- Storchi-Bergmann, T., Baldwin, J. & Wilson, A. 1993, *ApJ*, 410, L11
- Sulentic, J.W. & Marziani, P. 1999, *ApJ*, 518, L9
- Sulentic, J.W., et al. 1995, *ApJ*, 438, L1
- Sulentic, J.W., et al. 1998, *ApJ*, 501, 54
- Turnshek, D. et al. 1994, *ApJ*, 428, 93

Ulrich, M-H. 2000, A&ApRev, in press

Wang, T., Brinkmann, W., Bergeron, J. 1996, A&Ap, 309, 81

Yuan, W., Siebert, J. & Brinkmann, W. 1998, A&Ap, 334, 498

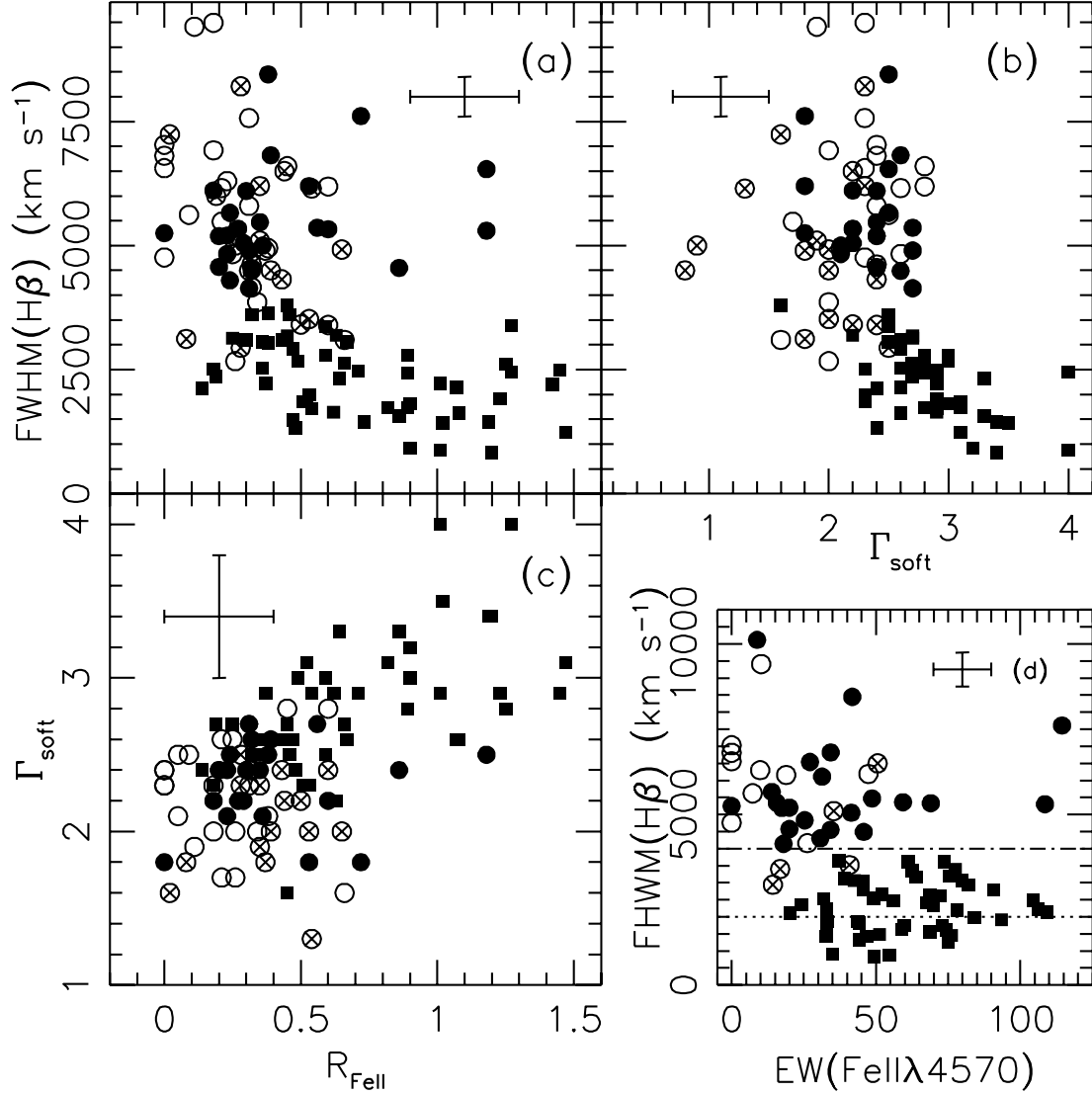


Fig. 1.— Panels a,b,c: The three principal correlation planes of Eigenvector 1. Solid symbols are radio-quiet sources (boxes: Pop. A, circles: Pop. B). Open symbols are radio-loud sources (open: core dominated, crossed: lobe dominated). Panel d: the BG92 sample plotted in the $W(\text{FeII } \lambda 4570)$ vs. $\text{FWHM}(\text{H}\beta_{\text{BC}})$ plane. The dotted line at 2000 km s^{-1} separates NLSy1 and the rest of the sample, while the dot-dashed line at 4000 km s^{-1} sets the limit between Pop. A and Pop. B. Error bars indicate 2σ uncertainties for a “typical”, non-pathological data point at $\text{FWHM}(\text{H}\beta_{\text{BC}}) \approx 4000 \text{ km s}^{-1}$, $R_{\text{FeII}} \approx 0.5$, and error on Γ_{soft} equal to the median of errors for which Γ_{soft} was available.

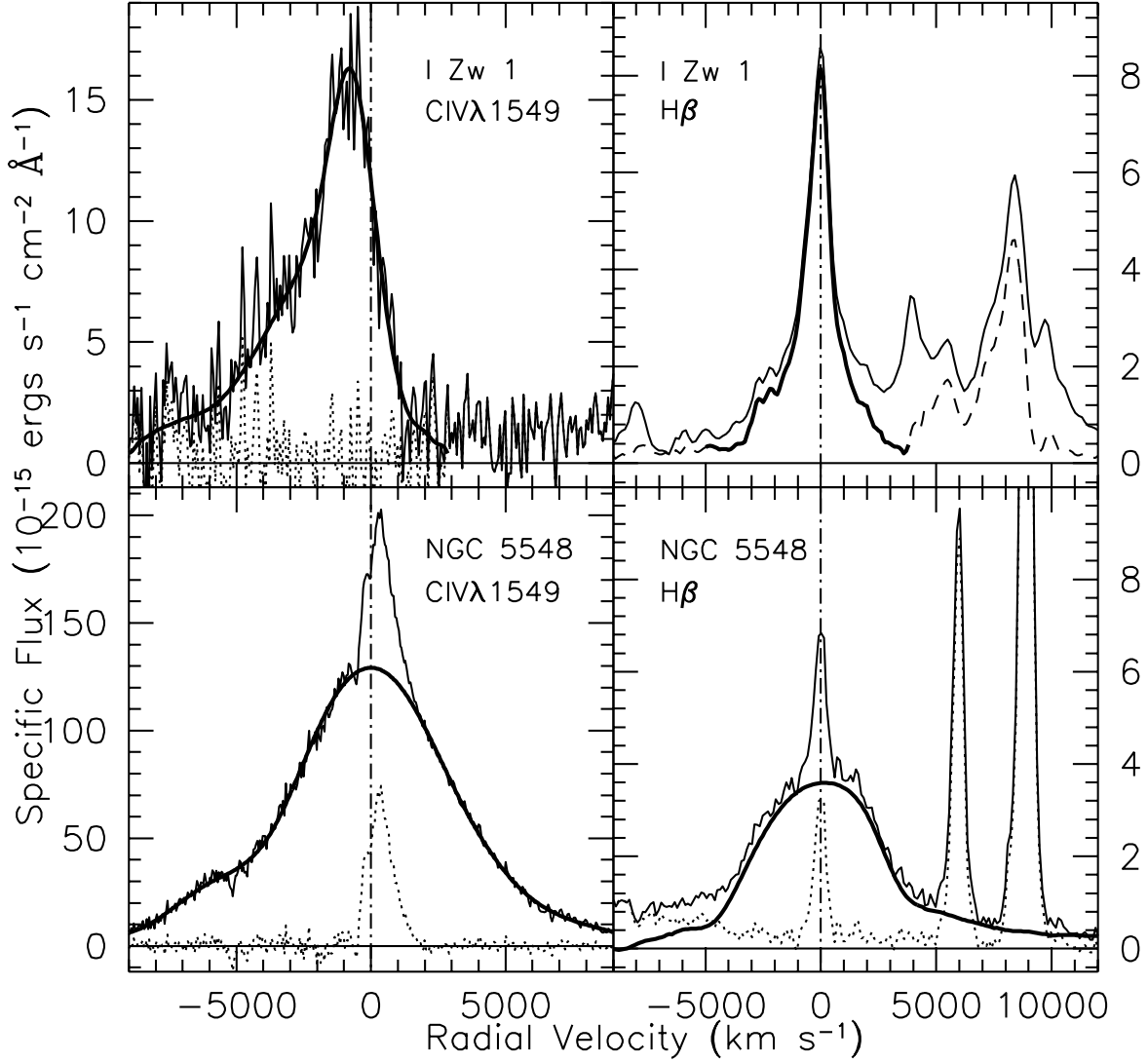


Fig. 2.— $H\beta$ (right panels; solid line: $H\beta_{BC}$) and $CIV\lambda 1549$ (left panels) broad line profiles for NLSy1 source I Zw 1 (“extreme” Pop. A, upper half) and Pop. B Seyfert 1 source NGC5548 (lower half). Note that the abscissa origin of I Zw 1 has been set by HI 21 cm measures. $[OIII]\lambda 5007$ lines show an appreciable blueshift with respect to the HI reference radial velocity as well as to the peak of the $H\beta$ profile. Dotted lines: residuals after broad component (thick line subtraction). Dashed line in I Zw 1 $H\beta$ panel: residual spectrum after $FeII_{opt}$ subtraction.

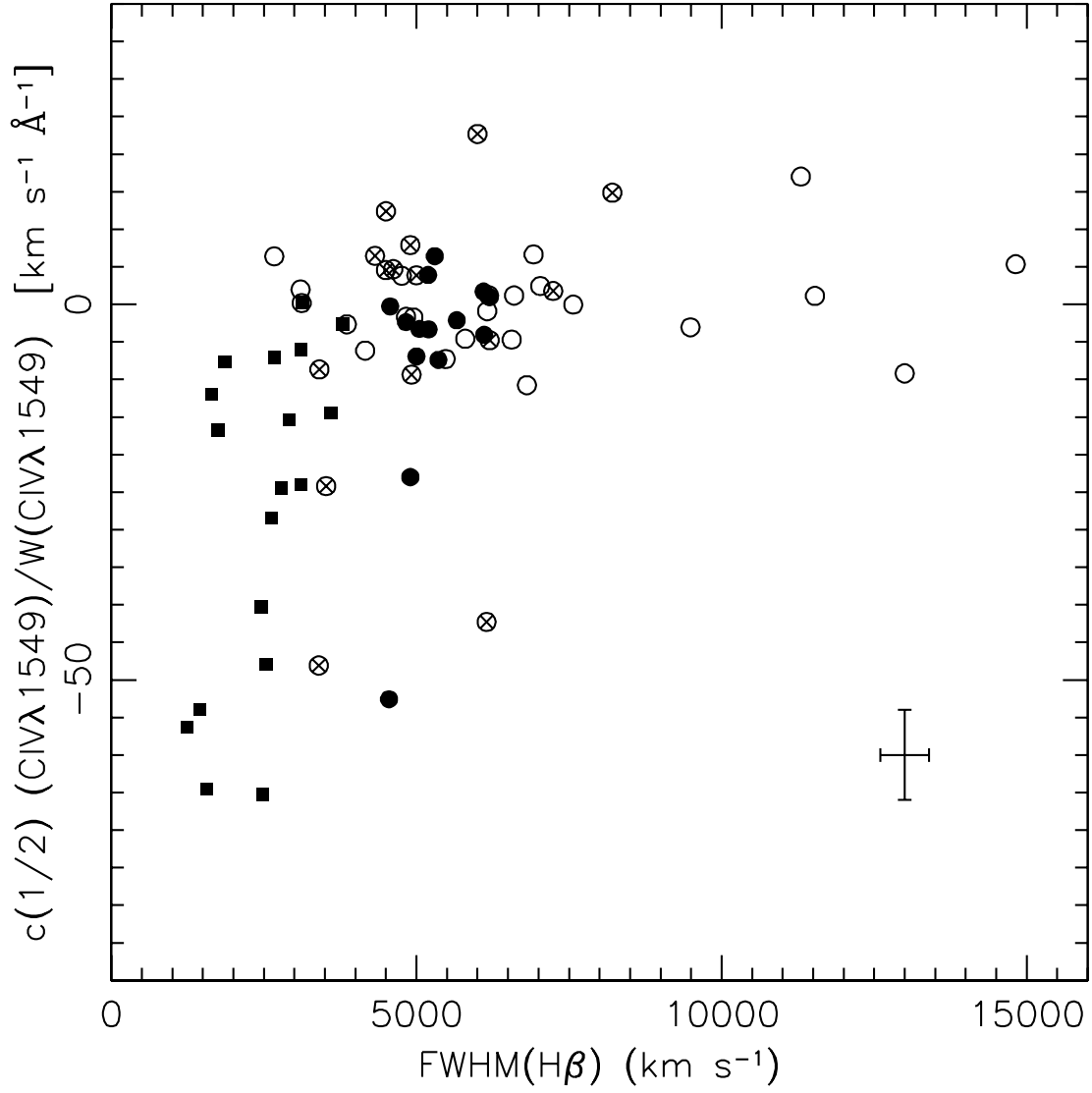


Fig. 3.— Relationships between $\text{FWHM}(\text{H}\beta_{\text{BC}})$ and $\text{CIV}\lambda 1549$ FWHM profile shift (blueshifts are negative) normalized by the rest-frame equivalent width of $\text{CIV}\lambda 1549$, $W(\text{CIV}\lambda 1549)$. Error bars are indicative as in Fig. 1 and refer to $W(\text{CIV}\lambda 1549) \approx 75 \text{ \AA}$ and shift $\approx 400 \text{ km s}^{-1}$.

TABLE 1
 PROPERTIES OF AGN POPULATIONS

AGN Class	FWHM range [km s ⁻¹]	N	W(H β) [\AA]	W(FeII λ 4570) [\AA]	R _{FeII}	W([OIII] λ 5007) [\AA]	Γ_{soft}	N $_{\Gamma}$
RQ Pop. A	0–2000	20	72 \pm 28	57 \pm 18	0.85 \pm 0.29	15.5 \pm 12.0	3.0 \pm 0.44	18
RQ Pop. A	2–3000	19	103 \pm 36	65 \pm 27	0.74 \pm 0.42	27.0 \pm 38.0	2.8 \pm 0.37	18
RQ Pop. A	3–4000	14	121 \pm 39	55 \pm 17	0.50 \pm 0.25	24.0 \pm 23.0	2.45 \pm 0.31	11
All RQ Pop. A	\leq 4000	53	96 \pm 39	59 \pm 21.5	0.72 \pm 0.35	22.0 \pm 27.0	2.82 \pm 0.43	47
All RQ Pop. B	$>$ 4000	27	104 \pm 33	39 \pm 27	0.40 \pm 0.29	27.0 \pm 25.0	2.33 \pm 0.28	23
All RQ	–	80	99 \pm 37.5	52 \pm 25	0.61 \pm 0.37	23.5 \pm 26.0	2.66 \pm 0.45	70
CD RL	–	19	79 \pm 29.5	28 \pm 17.5	0.36 \pm 0.16	20.0 \pm 11.5	2.06 \pm 0.73	19
LD RL	–	26	88 \pm 39	16.5 \pm 14.0	0.22 \pm 0.18	25.0 \pm 17.0	2.25 \pm 0.33	23
RL	\leq 4000	8	68.5 \pm 36	24 \pm 13	0.41 \pm 0.20	13.0 \pm 8.0	2.06 \pm 0.30	8
RL	$>$ 4000	37	88 \pm 34	21 \pm 17	0.25 \pm 0.17	25.0 \pm 16.0	2.18 \pm 0.60	34
All RL	–	45	84 \pm 35	21.5 \pm 16.5	0.28 \pm 0.18	23.0 \pm 15.0	2.16 \pm 0.55	42

TABLE 2
E1 SAMPLE PEARSON'S CORRELATION COEFFICIENTS

Correlates	ALL			ALL RL			ALL RQ			P	
	N	r_P	P	N	r_P	P	N	r_P	P	N	r_P
FWHM($H\beta$) vs. R_{FeII}	125	-0.50	$\lesssim 10^{-5}$	45	-0.37	0.01	80	-0.44	4×10^{-5}	47	-0.4
FWHM($H\beta$) vs. Γ	112	-0.41	1×10^{-5}	42	0.11	0.49	70	-0.63	$\lesssim 10^{-5}$	47	-0.5
Γ_{soft} vs. R_{FeII}	112	0.40	1×10^{-5}	42	-0.21	0.18	70	0.58	$\lesssim 10^{-5}$	47	-0.5
FWHM($H\beta$) vs. $v_r(\text{CIV})$	70	0.145	0.23	39	-0.15	0.36	31	0.19	0.30	18	-0.6
R_{FeII} vs. $v_r(\text{CIV})$	70	-0.52	1×10^{-5}	39	0.09	0.59	31	-0.62	2×10^{-4}	18	-0.5
Γ_{soft} vs. $v_r(\text{CIV})$	65	-0.20	0.10	37	0.09	0.60	28	-0.40	0.35	16	-0.3
W($H\beta$) vs. W(CIV)	72	0.31	0.009	39	0.23	0.16	33	0.46	0.007	19	0.4